Estimation of crop gross primary production (GPP): I. impact of MODIS observation footprint and impact of vegetation BRDF characteristics

Qingyuan Zhang [a,b,∗], Yen-Ben Cheng [c,b], Alexei I. Lyapustin [d], Yujie Wang [e,b], Xiangming Xiao [f], Andrew Suyker [g], Shashi Verma [g], Bin Tan [h], Elizabeth M. Middleton [b]

[a] Unversities Space Research Association, Columbia, MD 21044, USA
[b] Biospheric Sciences Laboratory, Code 618, National Aeronautics and Space Administration/Goddard Space Flight Center, Greenbelt, MD 20771, USA
[c] Earth Resources Technology, Inc. , Laurel, MD 20707, USA
[d] Climate and Radiation Laboratory, Code 613, National Aeronautics and Space Administration/Goddard Space Flight Center, Greenbelt, MD 20771, USA
[e] Goddard Earth Sciences and Technology Center, University of Maryland Baltimore County, Baltimore, MD 21228, USA
[f] Center for Spatial Analysis, University of Oklahoma, Norman, OK 73019, USA
[g] School of Natural Resources, University of Nebraska—Lincoln, Lincoln, NE 68588, USA
[h] Sigma Space Corporation, Lanham, MD 20706 USA

A R T I C L E   I N F O

A B S T R A C T

Accurate estimation of gross primary production (GPP) is essential for carbon cycle and climate change studies. Three AmeriFlux crop sites of maize and soybean were selected for this study. Two of the sites were irrigated and the other one was rainfed. The normalized difference vegetation index (NDVI), the enhanced vegetation index (EVI), the green band chlorophyll index (CI_{green}), and the green band wide dynamic range vegetation index ($WDRVI_{green}$) were computed from the moderate resolution imaging spectroradiometer (MODIS) surface reflectance data. We examined the impacts of the MODIS observation footprint and the vegetation bidirectional reflectance distribution function (BRDF) on crop daily GPP estimation with the four spectral vegetation indices (VIs - NDVI, EVI, $WDRVI_{green}$ and CI_{green}) where GPP was predicted with two linear models, with and without offset: $GPP = a \times VI \times PAR$ and $GPP = a \times VI \times PAR + b$. Model performance was evaluated with coefficient of determination (R^2), root mean square error (RMSE), and coefficient of variation (CV). The MODIS data were filtered into four categories and four experiments were conducted to assess the impacts. The first experiment included all observations. The second experiment only included observations with view zenith angle (VZA) $\leq 35°$ to constrain growth of the footprint size, which achieved a better grid cell match with the agricultural fields. The third experiment included only forward scatter observations with VZA $\leq 35°$. The fourth experiment included only backscatter observations with VZA $\leq 35°$. Overall, the EVI yielded the most consistently strong relationships to daily GPP under all examined conditions. The model $GPP = a \times VI \times PAR + b$ had better performance than the model $GPP = a \times VI \times PAR$, and the offset was significant for most cases. Better performance was obtained for the irrigated field than its counterpart rainfed field. Comparison of experiment 2 vs. experiment 1 was used to examine the observation footprint impact whereas comparison of experiment 4 vs. experiment 3 was used to examine the BRDF impact. Changes in R^2, RMSE, CV and changes in model coefficients "a" and "b" (experiment 2 vs. experiment 1; and experiment 4 vs. experiment 3) were indicators of the impacts. The second experiment produced better performance than the first experiment, increasing R^2 ($\uparrow 0.13$) and reducing RMSE ($\downarrow 0.68\,g\,C\,m^{-2}\,d^{-1}$) and CV ($\downarrow 9\%$). For each VI, the slope of $GPP = a \times VI \times PAR$ in the second experiment for each crop type changed little while the slope and intercept of $GPP = a \times VI \times PAR + b$ varied field by field. The CI_{green} was least affected by the MODIS observation footprint in estimating crop daily GPP (R^2, $\uparrow 0.08$; RMSE, $\downarrow 0.42\,g\,C\,m^{-2}\,d^{-1}$; and CV, $\downarrow 7\%$). Footprint most affected the NDVI (R^2, $\uparrow 0.15$; CV, $\downarrow 10\%$) and the EVI (RMSE, $\downarrow 0.84\,g\,C\,m^{-2}\,d^{-1}$). The vegetation BRDF impact also caused variation of model performance and change of model coefficients. Significantly different slopes were obtained for forward vs. backscatter observations, especially for the CI_{green} and the NDVI. Both the footprint impact and the BRDF impact varied with crop types, irrigation options, model options and VI options.

© 2014 Elsevier B.V. All rights reserved.

∗ Corresponding author at: Biospheric Sciences Laboratory, Code 618, NASA/Goddard Space Flight Center, Greenbelt, Maryland 20771, USA. Tel.: +1 301 614 6672.
E-mail address: qyz72@yahoo.com (Q. Zhang).

1. Introduction

Terrestrial carbon sequestration through vegetation photosynthesis (PSN) is essential for carbon cycle and climate change studies. The remote sensing data have been used to study PSN and to estimate gross primary production (GPP) for more than two decades (Potter et al., 1993; Randerson et al., 1996; Sellers et al., 1996; Sellers et al., 1986; Zhao and Running, 2010).

Two typical remote sensing approaches have been developed to estimate GPP. The first one is based on either the fraction of photosynthetically active radiation (PAR) absorbed for vegetation photosynthesis ($fAPAR_{PSN}$) or leaf area index for photosynthesis (LAI_{PSN}). The $fAPAR_{PSN}$ and LAI_{PSN} are derived from either physically-based models or empirical relationships with remote sensing vegetation indices (VIs) (Bonan et al., 2011; Fensholt et al., 2004; Field et al., 1995; Hall et al., 2008; Heinsch et al., 2006; Hember et al., 2010; Hilker et al., 2008; Hilker et al., 2011; Knyazikhin et al., 1999; Prince and Goward, 1996; Randall et al., 1996; Ruimy et al., 1999; Running et al., 2004; Waring et al., 2010; Xiao et al., 2004). For instance, the Simple Biosphere model (SiB) used the monthly normalized difference vegetation index (NDVI) from the Advanced Very High Resolution Radiometer (AVHRR) to estimate the fraction of PAR absorbed by a canopy ($fAPAR_{canopy}$) and to simulate GPP (Sellers et al., 1996; Sellers et al., 1986). The monthly AVHRR NDVI has also been ingested into the Carnegie-Ames-Stanford Approach (CASA) model to estimate terrestrial productivity (Potter et al., 1993; Randerson et al., 1996). The moderate resolution imaging spectrometer (MODIS) land science team has developed a standard global $fAPAR_{canopy}$ product (MOD15A2 FPAR) (Myneni et al., 2002) that is used as input in MOD17 global GPP algorithm (Zhao and Running, 2010). Xiao et al. (2004) proposed an 8-day Vegetation Photosynthesis Model (VPM) which assumed the fraction of PAR absorbed by the photosynthetic vegetation component (PV) for photosynthesis would be estimated by the enhanced vegetation index (Huete et al., 1997), i.e., the $fAPAR_{PV} = EVI$, $fAPAR_{PV}$ is also referred to as the fraction of PAR absorbed by chlorophyll ($fAPAR_{chl}$) (Jin et al., 2013; Kalfas et al., 2011). The second approach predicts GPP directly as the product of an empirical function of VI (f(VI)) and PAR: $GPP = f(VI) \times PAR$ (Cheng et al., 2009; Gitelson et al., 2012a; Gitelson et al., 2008; Gitelson et al., 2006; Middleton et al., 2009; Peng and Gitelson, 2011, 2012; Peng et al., 2010; Peng et al., 2011; Peng et al., 2013; Sakamoto et al., 2011; Wu et al., 2009). For example, Gitelson and his colleagues have utilized the green band chlorophyll index (CI_{green}) and the green band wide dynamic range vegetation index ($WDRVI_{green}$) derived from field measurements (Gitelson et al., 2006; Peng and Gitelson, 2011, 2012; Peng et al., 2011) and the Landsat data (Gitelson et al., 2012a; Gitelson et al., 2008) to estimate GPP with the function $GPP \alpha \propto VI \times PAR$. Note that some process models and machine learning models also involve remote sensing data in GPP simulation (Moffat et al., 2010; Potter et al., 2009; Xiao et al., 2010; Yang et al., 2007) that are beyond the scope of this study.

There is no existing literature that presents quantitative analysis of the impact of MODIS observation footprint and the impact of vegetation bidirectional reflectance distribution function (BRDF) characteristics on estimation of crop daily GPP. The footprint of a MODIS L1B observation (MOD021KM and MOD02HKM) is the area it actually covers. MODIS is a whiskbroom sensor and the MODIS observation footprint size grows with the view zenith angle (VZA) while the grid cell dimension remains fixed (Wolfe et al., 1998). One MODIS L1B observation may overlap with multiple grids, and a grid may overlap with multiple MODIS L1B observations from a single swath. The gridded MODIS MOD09 surface reflectance products have been widely applied in GPP estimation (Jin et al., 2013; Kalfas et al., 2011; Peng et al., 2013; Sims et al., 2008; Xiao et al., 2004; Zhao

and Running, 2010). In the gridding process to produce the standard MOD09 products, "Rather than discard multiple observations of the same location, . . . all observations that fall over a significant portion of each output geolocated grid cell are stored" (Wolfe et al., 1998). This means, for any given grid of the standard MOD09 products, (1) the footprint sizes and locations of observations used to grid for this grid cell vary with viewing geometries; (2) the footprints do not necessarily always have common area or overlap each other; and (3) the footprints do not always completely cover the grid. This footprint study is different from the study of climatology footprint analysis (Chen et al., 2012) which focused on climatology modeling aspect of variable footprints. We used a modified gridding approach in this study to process MODIS bands 1–7 data (see Section 2) and examined the impacts on daily GPP estimation of (1) the MODIS observation footprint and (2) the vegetation BRDF, for two crop types (maize, soybean) using four vegetation indices (VIs) (NDVI, EVI, $WDRVI_{green}$ and CI_{green}). The VIs were coupled with two linear models, $GPP = a \times VI \times PAR$ and $GPP = a \times VI \times PAR + b$, also referred to as greenness and radiation models (GR) (Gitelson et al., 2006; Wu et al., 2011).

2. Methods

We selected three AmeriFlux crop sites to investigate the impact of MODIS observation footprint and the impact of vegetation BRDF characteristics on crop daily GPP estimation from space. These crop sites are located at the University of Nebraska–Lincoln (UNL) Agricultural Research and Development Center near Mead, Nebraska (US-NE1, US-NE2 and US-NE3). The US-NE1 site (41°09′54.2″N, 96°28′35.9″W) and US-NE2 site (41°09′53.6″N, 96°28′07.5″W) are two circular fields (radius ∼ 390 m) and the US-NE3 site (41°10′46.7″N, 96°26′22.4″W) is a square field (length ∼ 790 m). The first two fields are equipped with center-pivot irrigation systems while the third field relies entirely on rainfall. Each field is equipped with an eddy covariance flux tower (Gitelson et al., 2008; Peng et al., 2013). The first field has a continuous maize (*Zea mays* L.) planting scheme while the other two fields are maize-soybean (*Glycine max* [L.] Merr.) rotation fields (maize, planted in odd years). The PAR and GPP data acquired at the towers are publically available and can be downloaded from ftp://cdiac.ornl.gov/pub/ameriflux/data/. The nighttime ecosystem respiration/temperature Q_{10} relationship was used to estimate the daytime ecosystem respiration. Daily GPP was computed by subtracting respiration (R) from net ecosystem exchange (NEE), i.e., $GPP = NEE-R$ (Suyker et al., 2005). These sites provide us an opportunity to examine these impacts on different vegetation types (C3 vs. C4 crops) in both irrigated and non-irrigated ecosystems.

MODIS L1B calibrated radiance data (MOD021KM and MOD02HKM) and geolocation data (MOD03) were downloaded from https://ladsweb.nascom.nasa.gov:9400/data/. Two of the MODIS bands have nadir spatial resolution of 250 m: B1 (red, 620–670 nm) and B2 (near infrared, NIR_1, 841–876 nm). The MODIS land bands 3–7 have nadir spatial resolution of 500 m: B3 (blue, 459–479 nm), B4 (green, 545–565 nm), B5 (NIR_2, 1230–1250 nm), B6 (shortwave infrared, $SWIR_1$, 1628–1652 nm) and B7 ($SWIR_2$, 2105–2155 nm). Other MODIS bands have nadir spatial resolution of 1 km. The centers of the original 500 m grids defined in the standard MOD09 products (Wolfe et al., 1998) that encompass the three tower sites are not the centers of the fields, and the mismatches may increase uncertainty in applications of the MOD09 products [please check the Fig. 2 in (Guindin-Garcia et al., 2012) for details]. Therefore a modified gridding approach was used in this study and we defined the centers of the three fields as centers of three 500 m grids. In the modified gridding process, the L1B radiance data from each swath were then gridded

at 500 m resolution for MODIS bands 1–7 and 1 km resolution for the other bands with area weights of each MODIS observation. This gridding approach ensures, for a given grid, that it is fully covered by the observations from each swath and there is only one gridded MODIS observation from the swath. This modified gridding processing was included in the Multi-Angle Implementation of Atmospheric Correction (MAIAC) algorithm (Lyapustin et al., 2011a; Lyapustin et al., 2008; Lyapustin et al., 2012; Lyapustin et al., 2011b). MAIAC is an advanced algorithm which uses time series analysis and a combination of pixel-based and image-based processing to improve accuracy of cloud/snow detection, aerosol retrievals, and atmospheric correction by incorporating the BRDF model of surface.

The bidirectional reflectance factors (BRF, also called surface reflectance) in MODIS bands 1–7 derived using the MAIAC algorithm were used in this study. The surface reflectance data (ρ) were used to calculate the following indices for further analysis (Deering, 1978; Gitelson et al., 2012b; Gitelson et al., 2005; Huete et al., 2002; Huete et al., 1997; Tucker, 1979):

$$CI_{green} = \frac{\rho_{NIR1}}{\rho_{green}} - 1 \tag{1}$$

$$WDRVI_{green} = \frac{0.3\rho_{NIR1} - \rho_{green}}{0.3\rho_{NIR1} + \rho_{green}} + \frac{1 - 0.3}{1 + 0.3} \tag{2}$$

$$NDVI = \frac{\rho_{NIR1} - \rho_{red}}{\rho_{NIR1} + \rho_{red}} \tag{3}$$

$$EVI = 2.5 \frac{\rho NIR_1 - \rho_{red}}{1 + \rho NIR_1 + 6\rho_{red} - 7.5\rho_{blue}} \tag{4}$$

The products of MODIS vegetation indices (VIs) and daily PAR (VI × PAR) were computed and compared against the tower based daily GPP. For each VI, we tested two linear models with and without offset: $y = ax$ and $y = ax + b$, where y = GPP, x = VI × PAR, the coefficients "a" and "b" were computed with the least squares best fit algorithm. To assess the impact of MODIS observation footprint and the impact of vegetation BRDF characteristics on crop daily GPP estimation, the data were filtered into four categories and four experiments were conducted. The first experiment included all observations. The second experiment included only observations with view zenith angle (VZA) $\leq 35°$ to constrain the footprint size to achieve a better match with the agricultural fields, and their plant functional types. The third experiment included only the observations in the forward scatter direction (relative azimuth angle, RAA > 90°) from the second experiment. The fourth experiment included only observations in the back scatter direction (RAA > 90°) from experiment two. Comparison of experiment 2 vs. experiment 1 was used to examine the observation footprint impact whereas comparison of experiment 4 vs. experiment 3 was used to examine the BRDF impact. In summary, we tested thirty-two cases in total (four vegetation indices, two regression models, four experiments) for the product of VI and PAR versus daily GPP acquired at the towers for two crop types in three fields. Coefficient of determination (R^2), root mean square error (RMSE), and coefficient of variation (CV) are reported to evaluate model performance. Changes in R^2, RMSE, CV and changes in model coefficients "a" and "b" (experiment 2 vs. experiment 1; and experiment 4 vs. experiment 3) were indicators of the impacts on daily GPP estimation.

3. Results

Maize was planted in US-NE1 in all years and in US-NE2 and US-NE3 in odd years. Soybean was planted in US-NE2 and US-NE3 in even years. Figs. 1–4 compare the product of VI and daily PAR versus daily GPP from tower fluxes for experiments 1–4 for maize in US-NE1. The x intercepts of the model y=ax+b give the

Table 1
Fit-function relationships (US-NE1, maize): tower based VI × PAR vs. GPP. Columns 3–6 summarize for the function y=ax and columns 7–10 summarize for the function y=ax+b, where y is tower flux based GPP and x is VI × PAR (VIs are NDVI, EVI, WDRVI_green and CI_green). Fit function, determination coefficient (R^2), root mean square deviation (RMSE, g C m⁻² d⁻¹) and coefficient of variation (CV, %) of each are presented. The most successful model in each group is designated with bold text.

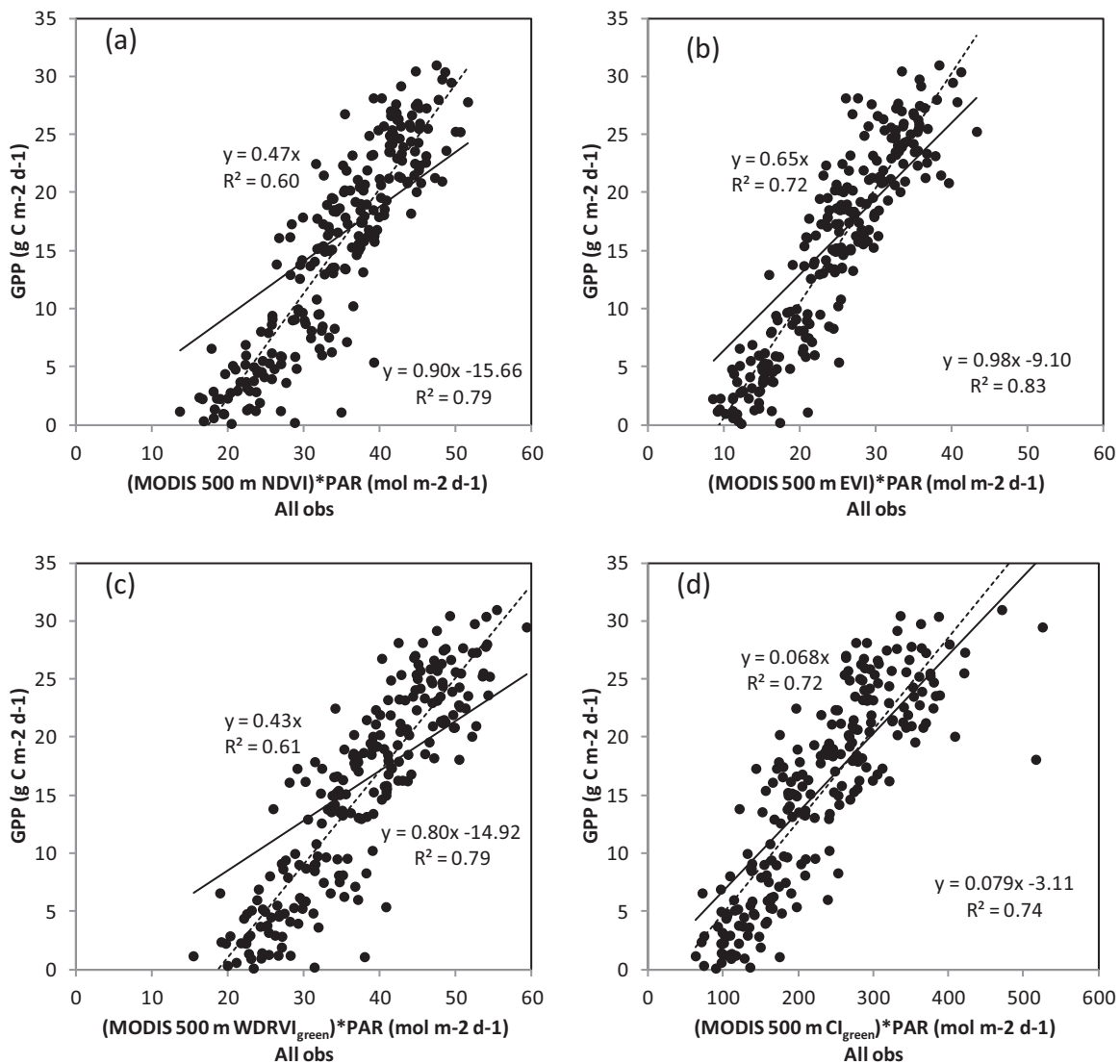|		NDVI y = ax	EVI	WDRVI_green	CI_green	NDVI y = ax + b	EVI	WDRVI_green	CI_green
All observations (experiment 1)	Fit-function	y=0.47x	y=0.65x	y=0.43x	y=0.068x	y=0.90x − 15.66	y=0.98x − 9.10	y=0.80x − 14.92	y=0.079x − 3.11
	R²	0.60	**0.72**	0.61	0.72	0.79	**0.83**	0.79	0.74
	RMSE	5.34	**4.44**	5.29	4.51	3.91	**3.57**	3.94	4.39
	CV	41%	**34%**	40%	34%	30%	**27%**	30%	33%
Observations (VZA ≤ 35°) (experiment 2)	Fit-function	y=0.48x	y=0.65x	y=0.44x	y=0.070x	y=0.89x − 14.86	y=0.93x − 7.80	y=0.8x − 14.32	y=0.081x − 2.97
	R²	0.67	**0.80**	0.67	0.78	0.86	**0.89**	0.85	0.79
	RMSE	4.85	**3.74**	4.88	4.05	3.20	**2.84**	3.35	3.90
	CV	31%	**24%**	31%	26%	21%	**18%**	22%	25%
Forward scatter observations (VZA ≤ 35°) (experiment 3)	Fit-function	y=0.46x	y=0.66x	y=0.42x	y=0.064x	y=0.92x − 16.37	y=0.97x − 8.21	y=0.80x − 15.07	y=0.077x − 3.59
	R²	0.64	0.80	0.66	**0.82**	0.87	**0.90**	0.87	0.84
	RMSE	5.11	3.84	5.02	**3.72**	3.10	**2.77**	3.21	3.45
	CV	33%	25%	32%	**24%**	20%	**18%**	21%	22%
Backscatter observations (VZA ≤ 35°) (experiment 4)	Fit-function	y=0.50x	y=0.65x	y=0.46x	y=0.076x	y=0.85x − 13.19	y=0.92x − 7.94	y=0.80x − 13.42	y=0.089x − 3.25
	R²	0.69	**0.81**	0.69	0.79	0.85	**0.89**	0.85	0.81
	RMSE	4.21	**3.52**	4.63	3.84	3.26	**2.82**	3.29	3.69
	CV	27%	**23%**	30%	25%	21%	**18%**	21%	24%

Fig. 1. Relationships between VI × (daily PAR) vs. tower flux daily GPP for the US-NE1 site: (1) NDVI × PAR vs. GPP; (2) EVI × PAR vs. GPP; (3) WDRVI$_{green}$ × PAR vs. GPP; and (4) CI$_{green}$ × PAR vs. GPP. The solid lines force intercepts to zero (upper eqns.) while dashed lines do not (lower eqns.). All observations are included.

minimum VI*PAR values at zero GPP on all charts (Figs. 1–4). In order to save pages, we do not present the similar figures for experiments 1–4 for maize/soybean in US-NE2/US-NE3 in this publication, but all the statistics for each crop type in each field were summarized in Tables 1–5. Tables 1, 2 and 4 list the slopes (coefficient "a", g C mol PPFD^{-1}) and intercepts (coefficient "b", g C m^{-2} d^{-1}) of the linear relationships ($y = ax$ and $y = ax + b$) of the thirty-two fit-functions for maize in fields US-NE1, US-NE2 and US-NE3 while Tables 3 and 5 report the slopes and intercepts of the thirty-two fit-functions for soybean in fields US-NE2 and US-NE3.

Daily GPP of maize, a C4 crop, ranged from ∼0–34 g C m^{-2} d^{-1} while daily GPP of soybean, a C3 crop, ranged from ∼ 0–19 g C m^{-2} d^{-1}. For each experiment, CI$_{green}$ has the widest range among the four VIs and EVI has the narrowest range. For instance, in Fig. 1, the ranges of NDVI, EVI, WDRVI$_{green}$ and CI$_{green}$ were 0.22–0.90, 0.13–0.75, 0.30–1.11, and 1.04–11.32, respectively. R^2, RSME and CV values in Tables 1–5 indicate the performance of the thirty-two cases of each crop type per field. In general, the model $y = ax + b$ yielded better performance (higher

R^2, lower RMSE and lower CV values) than $y = ax$ (Tables 1–5). Tables 1–5 show that the NDVI and WDRVI$_{green}$ are clearly inferior in estimating daily crop GPP. Tables 1–5 also present that, in experiment 1, EVI performs best in five groups and CI$_{green}$ performs best in the other five groups in aspects of R^2, RMSE and CV; in experiment 2, EVI performs best in nine groups while CI$_{green}$ performs best in the other one group; in experiment 3, EVI performs best in seven groups while CI$_{green}$ performs best in the other three groups; and, in experiment 4, EVI performs best in nine groups while CI$_{green}$ performs best in the other one group (see bold text in Tables 1–5).

3.1. Impact of MODIS observation footprint on crop daily GPP estimation (experiment 1 vs. experiment 2)

Comparison of experiments 1 vs. experiment 2 was used to show the impact of MODIS observation footprint on crop daily GPP estimation. The first experiment included all observations and the second experiment included only observations with VZA less than 35° (Tables 1–5). Changes in R^2, RMSE, CV, and changes in
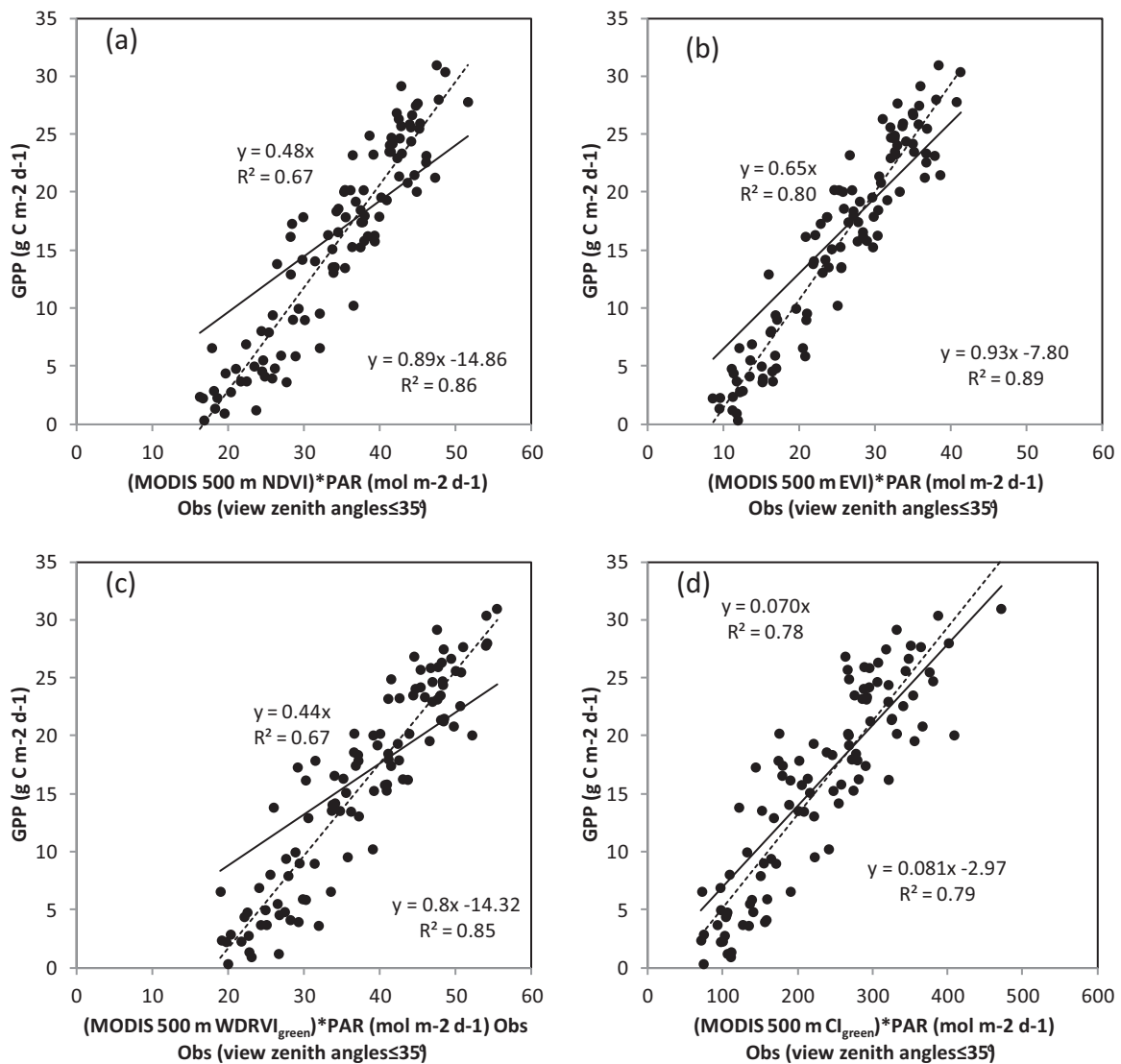
Fig. 2. Relationships between VI × (daily PAR) vs. tower flux daily GPP for the US-NE1 site: (1) NDVI × PAR vs. GPP; (2) EVI × PAR vs. GPP; (3) WDRVI$_{green}$ × PAR vs. GPP; and (4) CI$_{green}$ × PAR vs. GPP. The solid lines force intercepts to zero (upper eqns.) while dashed lines do not (lower eqns.). Only observations with view zenith angle less than 35° are included.

coefficients "a" and "b" of the models of experiment 1 vs. experiment 2 express the impact of footprint on daily crop GPP estimation. Minimum and maximum of changes in R^2, RMSE, CV, and coefficients "a" and "b" due to the MODIS observation footprint impact (experiment 2 – experiment 1) are listed in Table 6. The R2 values with CI$_{green}$ for the US-NE2 field do not change (Tables 2 and 6) from experiment 1 to experiment 2. All other cases of experiment 2 had higher R^2, lower RMSE and lower CV values than their counterpart cases of experiment 1 (Figs. 1–4 and Tables 1–6) (on average, R2, ↑0.13; RMSE, ↓0.68 g C m^{-2} d^{-1}; and CV, ↓9% in experiment 2).

The average changes in R^2, RMSE and CV due to the footprint impact on maize (Tables 1, 2 and 4) were less than the changes on soybean (Tables 3 and 5) (maize vs. soybean: R^2, ↑0.07 vs. ↑0.22; RMSE, ↓0.59 vs. ↓0.82 g C m^{-2} d^{-1}; and CV, ↓8% vs. ↓11%). The average changes in R^2 and RMSE due to the footprint impact in the irrigated fields US-NE1 and US-NE2 (Tables 1, 2, and 3) were less than the changes in the rainfed field US-NE3 (Tables 4 and 5) (irrigated vs. rainfed: R^2, ↑0.10 vs. ↑0.17; RMSE, ↓0.61 vs. ↓0.79 g C m^{-2} d^{-1}; and CV, ↓9% vs. ↓9%). The average changes in R^2, RMSE and CV

due to the footprint impact on the model y = ax were less than the changes on the model y = ax + b (Tables 1–5) (y = ax vs. y = ax + b: R^2, ↑0.11 vs. ↑0.14; RMSE, ↓0.58 vs. ↓0.78 g C m^{-2} d^{-1}; and CV, ↓8% vs. ↓10%). The average changes in R^2, RMSE and CV due to the footprint impact using CI$_{green}$ (R^2, ↑0.08; RMSE, ↓0.42 g C m^{-2} d^{-1}; and CV, ↓7%) were the least while the largest changes varied with VIs and terms (R^2: NDVI, ↑0.15; RMSE: EVI, ↓0.84 g C m^{-2} d^{-2}; and CV: NDVI ↓10%) (Tables 1–5).

Relative changes in coefficient "a" of the model y = ax due to the footprint impact were less than the relative changes in coefficient "a" of the model y = ax + b (Tables 1–5). The minimum and maximum values of relative changes in coefficient "a" of y = ax + b varied with VIs, field irrigation options and crop types. Changes in coefficient "b" for maize ranged from −1.4–2.6 g C m^{-2} d^{-1} while changes in coefficient "b" for soybean ranged from 0.2–6.3 g C m^{-2} d^{-1}. Changes in coefficient "b" also varied with field irrigation options and VI options (Tables 1–6). Overall, the footprint impact varied with crop types (maize < soybean), irrigation options (irrigated < rainfed), model options (model y = ax < model y = ax + b) and VI options (CI$_{green}$ < other VIs).
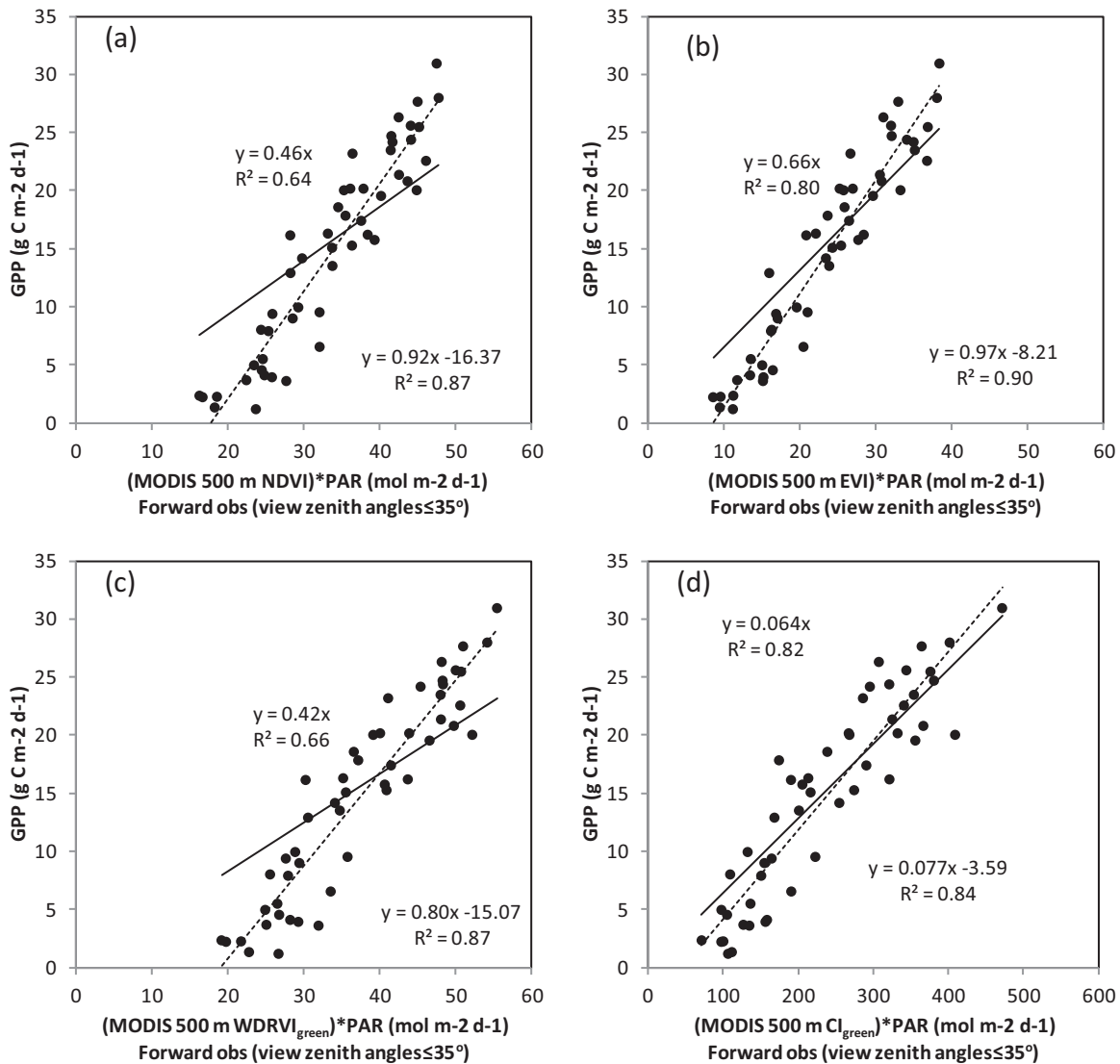
Fig. 3. Relationships between VI × (daily PAR) vs. tower flux daily GPP for the US-NE1 site: (1) NDVI × PAR vs. GPP; (2) EVI × PAR vs. GPP; (3) WDRVI$_{green}$ × PAR vs. GPP; and (4) CI$_{green}$ × PAR vs. GPP. The solid lines force intercepts to zero (upper eqns.) while dashed lines do not (lower eqns.). Only forward scatter observations with view zenith angle less than 35° are included.

3.2. Impact of vegetation BRDF characteristics on crop daily GPP estimation (experiment 3 vs. experiment 4)

The second experiment combines all observations with VZA less than 35° without distinguishing forward scatter/backscatter looking. The third experiment combined only the forward scatter observations in the second experiment while the fourth experiment combined only the backscatter observations.

Comparison of experiments 3 and 4 was used to show the impact of vegetation BRDF characteristics on crop daily GPP estimation (Tables 1–5). Minimum and maximum changes in R2, RMSE, CV, and coefficients "a" and "b" of the models due to the impact of vegetation BRDF characteristics were summarized in Table 7. Change in R^2 ranged from −0.15 to 0.12, change in RMSE: −0.90–0.65 g C m^{-2} d^{-1}, and change in CV: −22%–6%. Relative change in coefficient "a" of y = ax ranged from −6%–26%, relative change in coefficient "a" of y = ax + b: −36%–37%, and change in coefficient "b" of y = ax + b: −3.53–6.69 g C m^{-2} d^{-1}. Significantly different slopes were obtained for forward vs. back scatter observations, especially for the CI$_{green}$ and the NDVI (Tables 1–5). The

vegetation BRDF impact varied with crop types, irrigation options, model options and VI options (Table 7).

4. Discussion

The modified gridding procedure ensures (1) the centers of the grid cells match the centers of the fields and (2) the grid cells are completely covered by the observations from each swath data, which makes the gridded MODIS observations more appropriate for the footprint impact study than the standard MODIS gridded observations. Diameters of the two circular fields (US-NE1 and US-NE2, ~780 m) and length of the square field (US-NE3, ~790 m) are greater than the length of the 500 m grids. There is only one crop type at each field in each year, and is relatively homogeneous. Grass cover surrounding the study fields contributes to the worse performance of experiment 1 compared to experiment 2 since observations acquired at oblique angles are more likely to contain areas adjacent to the crop fields.

For both maize and soybean, almost all irrigated cases (Tables 2 and 3) from all of the four experiments had better
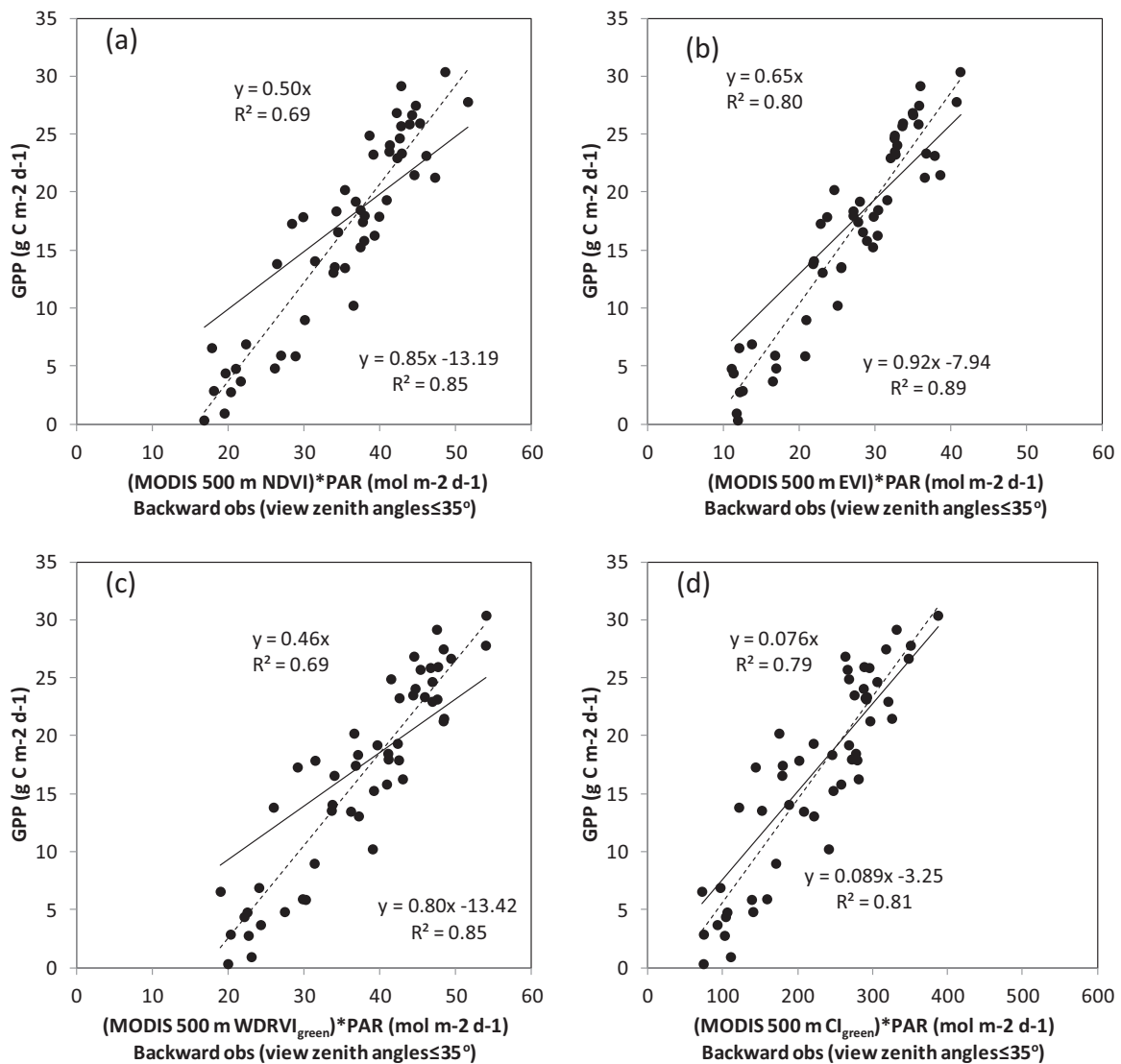
Fig. 4. Relationships between VI × (daily PAR) vs. tower flux daily GPP for the US-NE1 site: (1) NDVI × PAR vs. GPP; (2) EVI × PAR vs. GPP; (3) WDRVI$_{green}$ × PAR vs. GPP; and (4) CI$_{green}$ × PAR vs. GPP. The solid lines force intercepts to zero (upper eqns.) while dashed lines do not (lower eqns.). Only backscatter observations with view zenith angle less than 35° are included.

performances in terms of R^2, RMSE and CV than their counterpart rainfed cases (Tables 4 and 5). Vegetation in the irrigated field has less drought stress than in the rainfed field. Therefore the irrigated field is more favorable for vegetation photosynthesis and better model performance is obtained at the irrigated field than at the rainfed field.

For each VI, the slopes of the model $y = ax$ of the irrigated and the rainfed maize fields in the second experiment were very close to each other but with variable model performance (Tables 1, 2 and 4). For instance, the slopes of the model with EVI were 0.65, 0.66 and 0.67 for US-NE1, US-NE2 and US-NE3. The slopes of the model $y = ax$ of the irrigated and the rainfed soybean fields in experiment 2 were also very close to each other but with different model performance (Tables 3 and 5). For instance, the slopes of the model with EVI were 0.40 and 0.39 for US-NE2 and US-NE3. In contrast, the slope and intercept values of the counterpart $y = ax + b$ cases in experiment 2 varied field by field although the counterpart cases had better performance. For example, the fitted functions with EVI of the maize fields were: $y = 0.93x − 7.8$ (US-NE1), $y = 0.83x − 5.16$ (US-NE2), and $y = 0.94x − 6.56$ (US-NE3)

(Tables 1, 2 and 4). In experiment 2, the slope of $y = ax$ changed little for each crop type while the performance changed field by field; however, in order to achieve best prediction capability, the slope and intercept of $y = ax + b$ changed field by field even for the same crop type. Both models have advantages and disadvantages.

NDVI, EVI, WDRVI$_{green}$ and CI$_{green}$ were proposed for different purposes using data from a variety of sources by various scientists (Deering, 1978; Gitelson et al., 2012b; Gitelson et al., 2005; Huete et al., 2002; Huete et al., 1997; Tucker, 1979). NDVI, WDRVI$_{green}$ and CI$_{green}$ are two-band VIs, while EVI uses three spectral bands. The formulas of NDVI, WDRVI$_{green}$ and EVI include normalization while the CI$_{green}$ formula does not. In addition, the EVI formula has a factor that is designated to reduce soil/background impact while the other three do not. These differences among the formulas of the VIs contribute to the difference of their performance. Using MODIS red band WDRVI in GPP estimation may result in different performance from MODIS WDRVI$_{green}$, and with different impacts (personal communication, Anatoly A. Gitelson, University of Nebraska-Lincoln).

Table 2
Fit-function relationships (US-NE2, maize): tower based VI × PAR vs. GPP. Columns 3–6 summarize for the function $y = ax$ and columns 7–10 summarize for the function $y = ax + b$, where y is tower flux based GPP and x is VI × PAR (VIs are NDVI, EVI, WDRVI$_{green}$ and CI$_{green}$). Fit function, determination coefficient (R^2), root mean square deviation (RMSE, g C m^{-2} d^{-1}) and coefficient of variation (CV, %) of each are presented. The most successful model in each group is designated with bold text.

		NDVI $y = ax$	EVI	WDRVI$_{green}$	CI$_{green}$	NDVI $y = ax + b$	EVI	WDRVI$_{green}$	CI$_{green}$
All observations (experiment 1)	Fit-function	$y = 0.48x$	$y = 0.65x$	$y = 0.43x$	$y = 0.067x$	$y = 0.73x - 9.61$	$y = 0.86x - 6.02$	$y = 0.65x - 9.03$	$y = 0.070x - 0.69$
	R^2	0.64	**0.75**	0.65	0.72	0.74	**0.80**	0.74	0.72
	RMSE	5.04	**4.24**	5.00	4.49	4.33	**3.78**	4.35	4.48
	CV	36%	**30%**	36%	32%	31%	**27%**	31%	32%
Observations (VZA ≤ 35°) (experiment 2)	Fit-function	$y = 0.49x$	$y = 0.66x$	$y = 0.45x$	$y = 0.067x$	$y = 0.74x - 9.44$	$y = 0.83x - 5.16$	$y = 0.64x - 8.30$	$y = 0.064x + 0.71$
	R^2	0.72	**0.83**	0.71	0.72	0.81	**0.87**	0.79	0.72
	RMSE	4.38	**3.40**	4.42	4.39	3.58	**2.99**	3.79	4.38
	CV	26%	**20%**	27%	26%	22%	**18%**	23%	26%
Forward scatter observations (VZA ≤ 35°) (experiment 3)	Fit-function	$y = 0.48x$	$y = 0.66x$	$y = 0.43x$	$y = 0.061x$	$y = 0.77x - 11.32$	$y = 0.84x - 5.24$	$y = 0.64x - 9.13$	$y = 0.058x + 1.01$
	R^2	0.67	**0.82**	0.68	0.70	0.79	**0.86**	0.77	0.70
	RMSE	4.28	**3.17**	4.25	4.15	3.41	**2.78**	3.64	4.14
	CV	26%	**19%**	26%	25%	21%	**17%**	22%	25%
Backscatter observations (VZA ≤ 35°) (experiment 4)	Fit-function	$y = 0.50x$	$y = 0.65x$	$y = 0.46x$	$y = 0.074x$	$y = 0.72x - 8.51$	$y = 0.83x - 5.19$	$y = 0.66x - 8.12$	$y = 0.075\,x - 0.43$
	R^2	0.75	**0.83**	0.75	0.80	0.83	**0.88**	0.83	0.80
	RMSE	4.47	**3.62**	4.48	4.01	3.68	**3.17**	3.75	4.00
	CV	27%	**22%**	27%	24%	22%	**19%**	23%	24%

Table 3
Fit-function relationships (US-NE2, soybean): tower based VI × PAR vs. GPP. Columns 3–6 summarize for the function $y = ax$ and columns 7–10 summarize for the function $y = ax + b$, where y is tower flux based GPP and x is VI × PAR (VIs are NDVI, EVI, WDRVI$_{green}$ and CI$_{green}$). Fit function, determination coefficient (R^2), root mean square deviation (RMSE, g C m^{-2} d^{-1}) and coefficient of variation (CV, %) of each are presented. The most successful model in each group is designated with bold text.

		NDVI $y = ax$	EVI	WDRVI$_{green}$	CI$_{green}$	NDVI $y = ax + b$	EVI	WDRVI$_{green}$	CI$_{green}$
All observations (experiment 1)	Fit-function	$y = 0.30x$	$y = 0.40x$	$y = 0.28x$	$y = 0.043x$	$y = 0.40x - 3.66$	$y = 0.49x - 2.58$	$y = 0.36x - 3.23$	$y = 0.039x + 1.08$
	R^2	0.46	0.57	0.49	**0.61**	0.49	0.60	0.52	**0.62**
	RMSE	3.74	3.32	3.63	**3.18**	3.63	3.24	3.53	**3.16**
	CV	41%	37%	40%	**35%**	40%	36%	39%	**35%**
Observations (VZA ≤ 35°) (experiment 2)	Fit-function	$y = 0.31x$	$y = 0.40x$	$y = 0.28x$	$y = 0.042x$	$y = 0.52x - 7.78$	$y = 0.57x - 5.08$	$y = 0.44x - 6.30$	$y = 0.039x + 0.91$
	R^2	0.63	**0.75**	0.65	0.73	0.77	**0.83**	0.76	0.73
	RMSE	3.16	**2.61**	3.09	2.76	2.54	**2.16**	2.62	2.73
	CV	31%	**26%**	30%	27%	25%	**21%**	26%	27%
Forward scatter observations (VZA ≤ 35°) (experiment 3)	Fit-function	$y = 0.28x$	$y = 0.39x$	$y = 0.25x$	$y = 0.037x$	$y = 0.54x - 9.64$	$y = 0.62x - 6.59$	$y = 0.47x - 8.97$	$y = 0.040x - 0.84$
	R^2	0.63	0.74	0.67	**0.84**	0.84	0.88	**0.88**	0.85
	RMSE	3.37	2.81	3.15	**2.23**	2.26	1.95	**1.99**	2.20
	CV	38%	31%	35%	**25%**	25%	22%	**22%**	25%
Backscatter observations (VZA ≤ 35°) (experiment 4)	Fit-function	$y = 0.33x$	$y = 0.41x$	$y = 0.31x$	$y = 0.047x$	$y = 0.49x - 5.71$	$y = 0.51x - 3.22$	$y = 0.41x - 4.01$	$y = 0.039x + 2.20$
	R^2	0.67	**0.74**	0.68	0.69	0.75	**0.78**	0.73	0.73
	RMSE	2.73	**2.41**	2.69	2.64	2.39	**2.25**	2.49	2.50
	CV	24%	**22%**	24%	24%	21%	**20%**	22%	22%

Table 4

Fit-function relationships (US-NE3, maize): tower based VI × PAR vs. GPP. Columns 3–6 summarize for the function $y = ax$ and columns 7–10 summarize for the function $y = ax + b$, where y is tower flux based GPP and x is VI × PAR (VIs are NDVI, EVI, WDRVI$_{green}$ and CI$_{green}$). Fit function, determination coefficient (R^2), root mean square deviation (RMSE, g C m^{-2} d^{-1}) and coefficient of variation (CV, %) of each are presented. The most successful model in each group is designated with bold text.

		NDVI $y = ax$	EVI	WDRVI$_{green}$	CI$_{green}$	NDVI $y = ax + b$	EVI	WDRVI$_{green}$	CI$_{green}$
All observations (experiment 1)	Fit-function	$y = 0.43x$	$y = 0.63x$	$y = 0.41x$	$y = 0.073x$	$y = 0.66x - 7.87$	$y = 0.86x - 5.47$	$y = 0.61x - 7.53$	$y = 0.083x - 2.14$
	R^2	0.54	0.61	0.54	**0.64**	0.62	**0.66**	0.62	0.65
	RMSE	5.25	4.85	5.22	**4.66**	4.81	**4.56**	4.80	4.60
	CV	40%	37%	40%	**35%**	37%	**35%**	36%	35%
Observations (VZA ≤ 35°) (experiment 2)	Fit-function	$y = 0.45x$	$y = 0.67x$	$y = 0.43x$	$y = 0.076x$	$y = 0.75x - 10.47$	$y = 0.94x - 6.56$	$y = 0.69x - 9.78$	$y = 0.085x - 1.93$
	R^2	0.63	**0.70**	0.62	0.68	0.76	**0.78**	0.74	0.69
	RMSE	4.65	**4.14**	4.68	4.32	3.81	**3.65**	3.94	4.27
	CV	33%	**30%**	33%	31%	27%	**26%**	28%	31%
Forward scatter observations (VZA ≤ 35°) (experiment 3)	Fit-function	$y = 0.45x$	$y = 0.69x$	$y = 0.42x$	$y = 0.072x$	$y = 0.73x - 10.11$	$y = 0.95x - 6.10$	$y = 0.65x - 8.90$	$y = 0.074x - 0.67$
	R^2	0.62	**0.73**	0.62	0.67	0.74	**0.79**	0.72	0.68
	RMSE	4.43	**3.79**	4.46	4.17	3.69	**3.35**	3.87	4.16
	CV	31%	**27%**	31%	29%	26%	**23%**	27%	29%
Backscatter observations (VZA ≤ 35°) (experiment 4)	fit-function	$y = 0.46x$	$y = 0.65x$	$y = 0.44x$	$y = 0.081x$	$y = 0.77x - 10.84$	$y = 0.94x - 7.24$	$y = 0.74x - 10.98$	$y = 0.102x - 4.20$
	R^2	0.63	0.69	0.63	**0.72**	0.77	**0.78**	0.77	0.76
	RMSE	4.92	4.44	4.89	4.26	3.94	**3.84**	3.92	4.01
	CV	36%	32%	36%	**31%**	29%	**28%**	29%	29%

Table 5

Fit-function relationships (US-NE3, soybean): tower based VI × PAR vs. GPP. Columns 3–6 summarize for the function $y = ax$ and columns 7–10 summarize for the function $y = ax + b$, where y is tower flux based GPP and x is VI × PAR (VIs are NDVI, EVI, WDRVI$_{green}$ and CI$_{green}$). Fit function, determination coefficient (R^2), root mean square deviation (RMSE, g C m^{-2} d^{-1}) and coefficient of variation (CV, %) of each are presented. The most successful model in each group is designated with bold text.

		NDVI $y = ax$	EVI	WDRVI$_{green}$	CI$_{green}$	NDVI $y = ax + b$	EVI	WDRVI$_{green}$	CI$_{green}$
All observation (experiment 1)	Fit-function	$y = 0.28x$	$y = 0.39x$	$y = 0.26x$	$y = 0.044x$	$y = 0.40x - 4.31$	$y = 0.53x - 3.70$	$y = 0.34x - 3.22$	$y = 0.0420x + 0.45$
	R^2	0.29	0.41	0.31	**0.46**	0.33	0.45	0.34	**0.46**
	RMSE	4.06	3.69	4.00	**3.55**	3.97	3.59	3.94	**3.55**
	CV	44%	40%	44%	**39%**	43%	39%	43%	**39%**
Observations (VZA ≤ 35°) (experiment 2)	Fit-function	$y = 0.28x$	$y = 0.39x$	$y = 0.26x$	$y = 0.043x$	$y = 0.58x - 10.60$	$y = 0.62 x - 5.91$	$y = 0.48 x - 8.26$	$y = 0.043x + 0.00$
	R^2	0.50	0.63	0.52	**0.66**	0.69	**0.73**	0.66	0.66
	RMSE	3.35	2.88	3.29	**2.79**	2.67	**2.46**	2.79	2.79
	CV	36%	31%	36%	**30%**	29%	**27%**	30%	30%
Forward scatter observations (VZA ≤ 35°) (experiment 3)	Fit-function	$y = 0.25x$	$y = 0.38x$	$y = 0.23x$	$y = 0.041x$	$y = 0.61x - 12.35$	$y = 0.80x - 9.77$	$y = 0.53x - 11.17$	$y = 0.050x - 2.22$
	R^2	0.44	0.56	0.46	**0.67**	0.69	**0.79**	0.70	0.70
	RMSE	3.66	3.24	3.57	**2.81**	2.73	**2.27**	2.71	2.70
	CV	48%	42%	47%	**37%**	36%	**30%**	35%	35%
Backscatter observations (VZA ≤ 35°) (experiment 4)	Fit-function	$y = 0.31x$	$y = 0.40x$	$y = 0.29x$	$y = 0.045x$	$y = 0.51x - 7.39$	$y = 0.51x - 3.22$	$y = 0.40x - 4.47$	$y = 0.036x + 2.58$
	R^2	0.56	**0.64**	0.58	0.58	0.66	**0.67**	0.64	0.64
	RMSE	2.77	**2.51**	2.69	2.68	2.42	**2.40**	2.52	2.52
	CV	26%	**24%**	25%	25%	23%	**23%**	24%	24%

Table 6
Summary of the minimum and maximum changes in R², RMSE, CV, coefficients "a" and "b" due to the impact of MODIS observation footprint on crop daily GPP estimation (experiment 1 vs. experiment 2).

		Change in R^2		Change in RMSE		Change in CV		Relative change in "a" ($y = ax$)		Relative change in "a" ($y = ax + b$)		Change in "b" ($y = ax + b$)	
		Min	Max	Min	Max	Min	Max	Min	Max	Min	Max	Min	Max
Crop types	Maize	No change	0.14	−0.99	−0.10	−10%	−4%	−1%	6%	−8%	14%	−1.40	2.60
	Soybean	0.12	0.36	−1.30	−0.42	−15%	−8%	−2%	1%	−1%	44%	0.17	6.29
Irrigation options	Irrigated	No change	0.28	−1.10	−0.10	−15%	−6%	−2%	3%	−8%	28%	−1.40	4.12
	Non-irrigated	0.04	0.36	−1.30	−0.34	−14%	−4%	−1%	6%	3%	44%	−0.21	6.29
Model offset options	$y = ax$	No change	0.21	−0.83	−0.10	−11%	−5%	−2%	6%	NA	NA	NA	NA
	$y = ax + b$	No change	0.36	−1.30	−0.10	−15%	−4%	NA	NA	−8%	44%	−1.40	6.29
VI options	NDVI	0.07	0.36	−1.30	−0.48	−15%	−7%	1%	4%	−1%	44%	−0.77	6.29
	EVI	0.07	0.28	−1.12	−0.70	−15%	−7%	−1%	6%	−5%	16%	−1.30	2.50
	WDRVI$_{green}$	0.05	0.32	−1.15	−0.41	−13%	−6%	1%	5%	−2%	39%	−0.72	5.04
	CI$_{green}$	No change	0.20	−0.76	−0.10	−8%	−4%	−2%	4%	−8%	3%	−1.40	0.45

Table 7
Summary of the minimum and maximum changes in R², RMSE, CV, coefficients "a" and "b" due to the impact of vegetation BRDF characteristics on crop daily GPP estimation (experiment 3 vs. experiment 4).

		Change in R^2		Change in RMSE		Change in CV		Relative change in "a" ($y = ax$)		Relative change in "a" ($y = ax + b$)		Change in "b" ($y = ax + b$)	
		Min	Max	Min	Max	Min	Max	Min	Max	Min	Max	Min	Max
Crop types	Maize	−0.04	0.11	−0.90	0.65	−6%	6%	−6%	20%	−8%	37%	−3.53	3.21
	Soybean	−0.15	0.12	−0.89	0.50	−22%	No change	5%	26%	−36%	−3%	3.04	6.69
Irrigation options	Irrigated	−0.15	0.11	−0.90	0.50	−13%	3%	−2%	26%	−18%	30%	−1.44	4.95
	Non-irrigated	−0.12	0.12	−0.89	0.65	−22%	6%	−6%	24%	−36%	37%	−3.53	6.69
Model offset options	$y = ax$	−0.15	0.12	−0.90	0.65	−22%	6%	−6%	26%	NA	NA	NA	NA
	$y = ax + b$	−0.15	0.11	−0.31	0.50	−13%	5%	NA	NA	−36%	37%	−3.53	6.69
VI options	NDVI	−0.09	0.12	−0.90	0.49	−22%	5%	2%	23%	−17%	5%	−0.73	4.96
	EVI	−0.12	0.08	−0.73	0.65	−19%	6%	−6%	7%	−36%	−1%	−1.15	6.55
	WDRVI$_{green}$	−0.15	0.12	−0.88	0.50	−21%	4%	5%	24%	−25%	14%	−2.08	6.69
	CI$_{green}$	−0.15	0.11	−0.18	0.41	−12%	2%	12%	26%	−29%	37%	−3.53	4.80

The values of any particular VI for same field may vary when determined from different sensors (Kim et al., 2010; Miura et al., 2006). For instance, the US-NE1 CI_{green} during 7/11–7/20 of 2001–2004 computed from the field measured surface reflectance provided by UNL (field CI_{green}: 9.6–11.4) (Gitelson et al., 2006) was greater than the CI_{green} of the same field at the same time period derived from MODIS surface reflectance (MODIS CI_{green}: 7.0–8.8). In other words, the coefficients of functions relating daily GPP and $CI_{green} \times PAR$ developed with the UNL field measurements may be different from those developed with MODIS data, with different performance in terms of R^2, RMSE and CV.

Many studies have been conducted to validate/evaluate the usefulness of MODIS VIs in estimation of GPP without considering the impacts addressed here (Peng et al., 2013; Sims et al., 2005; Sims et al., 2008; Sims et al., 2006; Turner et al., 2004; Turner et al., 2003; Xiao et al., 2004). It is critical to investigate both the MODIS observation footprint impact and the BRDF impact on GPP estimates. Unlike the managed sites in this study, natural ecosystems often consist of multiple plant functional types within a 500 m or larger field. One should consider whether a grid cell (location and size) can well represent the field surrounding a flux tower site when using MODIS data. We hope the service that provides "standard" MODIS ASCII subsets for the AmeriFlux sites (http://ameriflux.ornl.gov/) also offers the subsets using the modified gridding procedure for all the AmeriFlux sites soon, so that the impacts for other types of ecosystems can be investigated.

5. Conclusions

On one hand, surface reflectance and VIs of a grid cell may vary with MODIS VZA (Galvão et al., 2011; Sims et al., 2011). On the other hand, MODIS observation footprint size changes with VZA. Both grid location and grid size should be considered when applying MODIS data in GPP estimation. This study examined the impacts of MODIS observation footprint and the vegetation BRDF on crop daily GPP estimation using four VIs and the linear models with and without offset: $y = ax$ and $y = ax + b$. The performance of the model $y = ax + b$ was better than the model $y = ax$ in aspects of R^2, RMSE and CV, which is consistent with previous works (Cheng et al., 2010; Wu et al., 2011). The MODIS EVI has the greatest probability to perform best in experiment 2 among the four VIs for crop daily GPP estimation. The MODIS observation footprint can affect the performance of both models with any of the four VIs. The MODIS observation footprint has the least impact on crop daily GPP estimation when using CI_{green} while the largest impact changes with VIs and terms: R^2 (NDVI), RMSE (EVI) and CV (NDVI). The impact of MODIS observation footprint can be reduced by using the modified gridding procedure and excluding observations with large VZAs. The vegetation BRDF can affect the slopes and intercepts of the models and their performance. Both impacts varied with crop types, irrigation options, model options and VI options. One should use caution when s/he extrapolates a VI based GPP model developed for a specific circumstance to other circumstances.

VIs do not explicitly express physical meaning in the models $y = ax$ and $y = ax + b$. Many studies have tried to find empirical relationship between NDVI and $fAPAR_{canopy}$ (Fensholt et al., 2004; Goward and Huemmrich, 1992; Huemmrich and Goward, 1997; Justice et al., 1998; Myneni et al., 2002; Myneni and Williams, 1994; Sims et al., 2005; Wu et al., 2012). Our earlier studies utilized multiple 30 m and 60 m spectrally MODIS-like images simulated from EO-1 Hyperion images to explore correlation between $fAPAR_{chl}$ and EVI and found that they were strongly correlated (Zhang et al., 2013; Zhang et al., 2012). Exploration of linear relationships between the actual MODIS VIs and $fAPAR_{chl}$ ($fAPAR_{chl} = p_1 \times VI + p_2$) is under way and findings will be reported in another paper. We will also examine whether the relationships vary with fields, plant functional types and irrigation options.

References

Bonan, G.B., Lawrence, P.J., Oleson, K.W., Levis, S., Jung, M., Reichstein, M., Lawrence, D.M., Swenson, S.C., 2011. Improving canopy processes in the Community Land Model version 4 (CLM4) using global flux fields empirically inferred from FLUXNET data. J. Geophys. Res. 116, G02014.

Chen, B., Coops, N.C., Fu, D., Margolis, H.A., Amiro, B.D., Black, T.A., Arain, M.A., Barr, A.G., Bourque, C.P.-A., Flanagan, L.B., Lafleur, P.M., McCaughey, J.H., Wofsy, S.C., 2012. Characterizing spatial representativeness of flux tower eddy-covariance measurements across the Canadian Carbon Program Network using remote sensing and footprint analysis. Rem. Sens. Environ. 124, 742–755.

Cheng, Y., Middleton, E.M., Hilker, T., Coops, N.C., Krishnan, P., Black, T.A., 2009. Dynamics of spectral bio-indicators and their correlations with light use efficiency using directional observations at a douglas-fir forest. Mesure. Sci. Technol. 20, 095–107.

Cheng, Y., Middleton, E.M., Huemmrich, K.F., Zhang, Q, Campbell, P., Corp, L.A., Russ, A.L., Kustas, W.P., 2010. Utilizing in situ directional hyperspectral measurements to validate bio-indicators for a corn crop canopy. Ecol. Inform. 5, 330–338.

Deering, D.W., 1978. Rangeland reflectance characteristics measured by aircraft and spacecraft sensors. In: College Station. Texas A&M University, TX, pp. 338.

Fensholt, R., Sandholt, I., Rasmussen, M.S., 2004. Evaluation of MODIS LAI, fAPAR and the relation between fAPAR and NDVI in a semi-arid environment using in situ measurements. Rem. Sens. Environ. 91, 490–507.

Field, C.B., Randerson, J.T., Malmstrom, C.M., 1995. Global net primary production - combining ecology and remote-sensing. Rem. Sens. Environ. 51, 74–88.

Galvão, L.S., Santos, J.R., Roberts, d., Breunig, D.A., Toomey, F.M., Moura, M.Y.M.d, 2011. On intra-annual EVI variability in the dry season of tropical forest: A case study with MODIS and hyperspectral data. Rem. Sens. Environ. 115, 2350–2359.

Gitelson, A.A., Peng, Y., Masek, J., Rundquist, D.C., Verma, S., Suyker, A., Baker, J.M., Hatfield, J., Meyers, T., 2012a. Remote estimation of crop gross primary production with Landsat data. Rem. Sens. Environ. 121, 404–414.

Gitelson, A.A., Peng, Y., Masek, J.G., Rundquist, D.C., Verma, S., Suyker, A., Baker, J.M., Hatfield, J.L., Meyers, T., 2012b. Remote estimation of crop gross primary production with Landsat data. Rem. Sens. Environ. 121, 404–414.

Gitelson, A.A., Viñá, A., Ciganda, s.V., Rundquist, n., Arkebauer, D.C.T.J., 2005. Remote estimation of canopy chlorophyll content in crops. Geophys. Res. Lett., 32.

Gitelson, A.A., Viña, A.J.G., Verma, M., Suyker, S.B.A.E., 2008. Synoptic monitoring of gross primary productivity of maize using landsat data. IEEE Geosci. Rem. Sens. Lett. 5, 133–137.

Gitelson, A.A., Viña, A., Verma, S.B., Rundquist, D.C., Arkebauer, T.J., Keydan, G., Leavitt, B., Ciganda, V., Burba, G.G., Suyker, A.E., 2006. Relationship between gross primary production and chlorophyll content in crops: Implications for the synoptic monitoring of vegetation productivity. J. Geophys. Res. 111, D08S11.

Goward, S.N., Huemmrich, K.F., 1992. Vegetation canopy PAR absorptance and the normalized difference vegetation index - an assessment using the SAIL Model. Rem. Sens. Environ. 39, 119–140.

Guindin-Garcia, N., Gitelson, A.A., Arkebauer, T.J., Shanahan, J., Weiss, A., 2012. An evaluation of MODIS 8- and 16-day composite products for monitoring maize green leaf area index. Agric. Forest Meteorol. 161, 15–25.

Hall, F.G., Hilker, T., Coops, N.C., Lyapustin, A., Huemmrich, K.F., Middleton, E., Margolis, H., Drolet, G., Black, T.A., 2008. Multi-angle remote sensing of forest light use efficiency by observing PRI variation with canopy shadow fraction. Rem. Sens. Environ. 112, 3201–3211.

Heinsch, F.A., Zhao, M., Running, S.W., Kimball, J.S., Nemani, R.R., Davis, K.J., Bolstad, P.V., Cook, B.D., Desai, A.R., Ricciuto, D.M., Law, B.E., Oechel, W.C., Kwon, H., Luo, H., Wofsy, S.C., Dunn, A.L., Munger, J.W., Baldocchi, D.D., Xu, L., Hollinger, D.Y., Richardson, A.D., Stoy, P.C., Siqueira, M.B.S., Monson, R.K., Burns, S.P., Flanagan, L.B., 2006. Evaluation of remote sensing based terrestrial productivity from MODIS using regional tower eddy flux network observations. IEEE Trans. Geosci. Rem. Sens. 44, 1908–1925.

Hember, R.A., Coops, N.C., Black, T.A., Guy, R.D., 2010. Simulating gross primary production across a chronosequence of coastal Douglas-fir forest stands with a production efficiency model. Agric. Forest Meteorol. 150, 238–253.

Hilker, T., Coops, N.C., Hall, F.G., Black, T.A., Wulder, M.A., Nesic, Z., Krishnan, P., 2008. Separating physiologically and directionally induced changes in PRI using BRDF models. Rem. Sens. Environ. 112, 2777–2788.

Hilker, T., Gitelson, A.A., Coops, N.C., Hall, F.G., Black, T.A., 2011. Tracking plant physiological properties from multi-angular tower-based remote sensing. Oecologia 165, 865–876.

Huemmrich, K.F., Goward, S.N., 1997. Vegetation canopy PAR absorptance and NDVI: An assessment for ten tree species with the SAIL model. Rem. Sens. Environ. 61, 254–269.

Huete, A., Didan, K., Miura, T., Rodriguez, E.P., Gao, X., Ferreira, L.G., 2002. Overview of the radiometric and biophysical performance of the MODIS vegetation indices. Rem. Sens. Environ. 83, 195–213.

Huete, A.R., Liu, H.Q., Batchily, K., vanLeeuwen, W., 1997. A comparison of vegetation indices global set of TM images for EOS-MODIS. Rem. Sens. Environ. 59, 440–451.

Jin, C., Xiao, X.M., Merbold, L., Arneth, A., Veenendaal, E., Kutsch, W., 2013. Phenology and gross primary production of two dominant savanna woodland ecosystems in Southern Africa. Rem. Sens. Environ. 135, 189–201.

Justice, C.O., Vermote, E., Townshend, J.R.G., Defries, R., Roy, D.P., Hall, D.K., Salomonson, V.V., Privette, J.L., Riggs, G., Strahler, A., Lucht, W., Myneni, R.B., Knyazikhin, Y., Running, S.W., Nemani, R.R., Wan, Z.M., Huete, A.R., van Leeuwen, W., Wolfe, R.E., Giglio, L., Muller, J.P., Lewis, P., Barnsley, M.J., 1998. The moderate resolution imaging spectroradiometer (MODIS): land remote sensing for global change research. IEEE Trans. Geosci. Rem. Sens. 36, 1228–1249.

Kalfas, J., Xiao, X., Vanegas, D., Verma, S., Suyker, A.E., 2011. Modeling gross primary production of irrigated and rain-fed maize using MODIS imagery and CO(2) flux tower data. Agric. Forest Meteorol. 151, 1514–1528.

Kim, Y., Huete, A.R., Miura, T., Jiang, Z., 2010. Spectral compatibility of vegetation indices across sensors: band decomposition analysis with Hyperion data. J. Appl. Rem. Sens. 4, 043520.

Knyazikhin, Y., Glassy, J., Privette, J.L., Tian, Y., Lotsch, A., Zhang, Y., Wang, Y., Morisette, J.T., Votava, P., Myneni, R.B., Nemani, R.R., & Running, S.W., 1999. MODIS leaf area index (LAI) and Fraction of photosynthetically active radiation absorbed by vegetation (FPAR) product (MOD15) Algorithm Theoretical Basis Document. http://modis.gsfc.nasa.gov/data/atbd/atbd_mod15.pdf

Lyapustin, A., Martonchik, J., Wang, Y., Laszlo, I., Korkin, S., 2011a. Multi-angle implementation of atmospheric correction (MAIAC): Part 1. radiative transfer basis and look-up tables. J. Geophys. Res. 116, D03210.

Lyapustin, A., Wang, Y., Frey, R., 2008. An automatic cloud mask algorithm based on time series of MODIS measurements. J. Geophys. Res. 113.

Lyapustin, A., Wang, Y., Laszlo, I., Hilker, T., Hall, F., Sellers, P., Tucker, J., Korkin, S., 2012. Multi-angle implementation of atmospheric correction for MODIS (MAIAC) 3: Atmospheric correction. Rem. Sens. Environ. 3 (127), 385–393.

Lyapustin, A., Wang, Y., Laszlo, I., Kahn, R., Korkin, S., Remer, L., Levy, R., Reid, J.S., 2011b. Multi-angle implementation of atmospheric correction (MAIAC): Part 2. aerosol algorithm. J. Geophys. Res. 116, D03211.

Middleton, E.M., Cheng, Y., Hilker, T., Black, T.A., Krishnan, P., Coops, N.C., Huemmrich, K.F., 2009. Linking foliage spectral responses to canopy level ecosystem photosynthetic light use efficiency at a Douglas-fir forest in Canada. Can. J. Rem. Sens. 35, 166–188.

Miura, T., Huete, A., Yoshioka, H., 2006. An empirical investigation of cross-sensor relationships of NDVI and red/near-infrared reflectance using EO-1 Hyperion data. Rem. Sens. Environ. 100, 223–236.

Moffat, A.M., Beckstein, C., Churkina, G., Mund, M., Heimann, M., 2010. Characterization of ecosystem responses to climatic controls using artificial neural networks. Glob. Change Biol. 16, 2737–2749.

Myneni, R.B., Hoffman, S., Knyazikhin, Y., Privette, J.L., Glassy, J., Tian, Y., Wang, Y., Song, X., Zhang, Y., Smith, G.R., Lotsch, A., Friedl, M., Morisette, J.T., Votava, P., Nemani, R.R., Running, S.W., 2002. Global products of vegetation leaf area and fraction absorbed PAR from year one of MODIS data. Rem. Sens. Environ. 83, 214–231.

Myneni, R.B., Williams, D.L., 1994. On the relationship between Fapar and Ndvi. Rem. Sens. Environ. 49, 200–211.

Peng, Y., Gitelson, A.A., 2011. Application of chlorophyll-related vegetation indices for remote estimation of maize productivity. Agric. Forest Meteorol. 151, 1267–1276.

Peng, Y., Gitelson, A.A., 2012. Remote estimation of gross primary productivity in soybean and maize based on total crop chlorophyll content. Rem. Sens. Environ. 117, 440–448.

Peng, Y., Gitelson, A.A., Keydan, G., Rundquist, D.C., Leavitt, B., Verma, S.B., Suyker, A.E., 2010. Remote estimation of gross primary production in Maize. In: Proceedings of 10th Int. Conference on Precision Agriculture, July 18–21, 2010, Denver, Colorado, USA, pp. 1–16, www.icpaonline.org.

Peng, Y., Gitelson, A.A., Keydan, G.P., Rundquist, D.C., Moses, W.J., 2011. Remote estimation of gross primary production in maize and support for a new paradigm based on total crop chlorophyll content. Rem. Sens. Environ. 115, 978–989.

Peng, Y., Gitelson, A.A., Sakamoto, T., 2013. Remote estimation of gross primary productivity in crops using MODIS 250 m data. Rem. Sens. Environ. 128, 186–196.

Potter, C., Klooster, S., Huete, A., Genovese, V., Bustamante, M., Ferreira Jr.R.C., L.G., Zepp, d.O.R., 2009. Terrestrial carbon sinks in the Brazilian Amazon and Cerrado region predicted from MODIS satellite data and ecosystem modeling. Biogeosciences 6, 937–945.

Potter, C.S., Randerson, J.T., Field, C.B., Matson, P.A., Vitousek, P.M., Mooney, H.A., Klooster, S.A., 1993. Terrestrial ecosystem production—a process model-based on global satellite and surface data. Global Biogeochem. Cycles 7, 811–841.

Prince, S.D., Goward, S.N., 1996. Evaluation of the NOAA/NASA Pathfinder AVHRR Land Data Set for global primary production modelling. Int. J. Rem. Sens. 17, 217–221.

Randall, D.A., Dazlich, D.A., Zhang, C., Denning, A.S., Sellers, P.J., Tucker, C.J., Bounoua, L., Los, S.O., Justice, C.O., Fung, I., 1996. A revised land surface parameterization (SiB2) for GCMs.III: The greening of the Colorado State University general circulation model. J. Climate 9, 738–763.

Randerson, J.T., Thompson, M.V., Malmstrom, C.M., Field, C.B., Fung, I.Y., 1996. Substrate limitations for heterotrophs: Implications for models that estimate the seasonal cycle of atmospheric CO_2. Global Biogeochem. Cycles 10, 585–602.

Ruimy, A., Kergoat, L., Bondeau, A., 1999. Comparing global models of terrestrial net primary productivity (NPP): analysis of differences in light absorption and light-use efficiency. Global Change Biol. 5, 56–64.

Running, S., Nemani, R., Heinsch, F., Zhao, M., Reeves, M., Hashimoto, H., 2004. A continuous satellite-derived measure of global terrestrial primary production. Bioscience 54, 547–560.

Sakamoto, T., Gitelson, A.A., Wardlow, B.D., Verma, S.B., Suyker, A.E., 2011. Estimating daily gross primary production of maize based only on MODIS WDRVI and shortwave radiation data. Rem. Sens. Environ. 115, 3091–3101.

Sellers, P.J., Los, S.O., Tucker, C.J., Justice, C.O., Dazlich, D.A., Collatz, G.J., Randall, D.A., 1996. A revised land surface parameterization (SiB2) for atmospheric GCMs.II: The generation of global fields of terrestrial biophysical parameters from satellite data. J. Climate 9, 706–737.

Sellers, P.J., Mintz, Y., Sud, Y.C., Dalcher, A., 1986. A Simple Biosphere Model (SIB) for use within general circulation models. J. Atmos. Sci. 43, 505–531.

Sims, D.A., Rahman, A.F., Cordova, V.D., Baldocchi, D.D., Flanagan, L.B., Goldstein, A.H., Hollinger, D.Y., Misson, L., Monson, R.K., Schmid, H.P., Wofsy, S.C., Xu, L.K., 2005. Midday values of gross CO_2 flux and light use efficiency during satellite overpasses can be used to directly estimate eight-day mean flux. Agric. Forest Meteorol. 131, 1–12.

Sims, D.A., Rahman, A.F., Cordova, V.D., El-Masri, B.Z., Baldocchi, D.D., Bolstad, P.V., Flanagan, L.B., Goldstein, A.H., Hollinger, D.Y., Misson, L., Monson, R.K., Oechel, W.C., Schmid, H.P., Wofsy, S.C., Xu, L., 2008. A new model of gross primary productivity for North American ecosystems based solely on the enhanced vegetation index and land surface temperature from MODIS. Rem. Sens. Environ. 112, 1633–1646.

Sims, D.A., Rahman, A.F., Cordova, V.D., El-Masri, B.Z., Baldocchi, D.D., Flanagan, L.B., Goldstein, A.H., Hollinger, D.Y., Misson, L., Monson, R.K., Oechel, W.C., Schmid, H.P., Wofsy, S.C., Xu, L., 2006. On the use of MODIS EVI to assess gross primary productivity of North American ecosystems. J. Geophys. Res. 111, 1–16.

Sims, D.A., Rahman, A.F., Vermote, E.F., Jiang, Z.N., 2011. Seasonal and inter-annual variation in view angle effects on MODIS vegetation indices at three forest sites. Rem. Sens. Environ. 115, 3112–3120.

Suyker, A.E., Verma, S.B., Burba, G.G., Arkebauer, T.J., 2005. gross primary production and ecosystem respiration of irrigated maize and irrigated soybean during a growing season. Agric. Forest Meteorol. 131, 180–190.

Tucker, C.J., 1979. Red and photographic infrared linear combinations for monitoring vegetation. Rem. Sens. Environ. 8, 127–150.

Turner, D.P., Ollinger, S., Smith, M.L., Krankina, O., Gregory, M., 2004. Scaling net primary production to a MODIS footprint in support of Earth observing system product validation. Int. J. Rem. Sens. 25, 1961–1979.

Turner, D.P., Ritts, W.D., Cohen, W.B., Gower, S.T., Zhao, M.S., Running, S.W., Wofsy, S.C., Urbanski, S., Dunn, A.L., Munger, J.W., 2003. Scaling Gross Primary Production (GPP) over boreal and deciduous forest landscapes in support of MODIS GPP product validation. Rem. Sens. Environ. 88, 256–270.

Waring, R.H., Coops, N.C., Landsberg, J.J., 2010. Improving predictions of forest growth using the 3-PGS model with observations made by remote sensing. Forest Ecol. Manage. 259, 1722–1729.

Wolfe, R., Roy, D., Vermote, E., 1998. The MODIS land data storage, gridding and compositing methodology: Level 2 Grid. IEEE Trans. Geosci. Rem. Sens. 36, 1324–1338.

Wu, C., Chen, J.M., Desai, A.R., Hollinger, D.Y., Arain, M.A., Margolis, H.A., Gough, C.M., Staebler, R.M., 2012. Remote sensing of canopy light use efficiency in temperate and boreal forests of North America using MODIS imagery. Rem. Sens. Environ. 118, 60–72.

Wu, C., Chen, J.M., Huang, N., 2011. Predicting gross primary production from the enhanced vegetation index and photosynthetically active radiation: Evaluation and calibration. Rem. Sens. Environ. 115, 3424–3435.

Wu, C., Niu, Z., Tang, Q., Huang, W., Rivard, B., Feng, J., 2009. Remote estimation of gross primary production in wheat using chlorophyll-related vegetation indices. Agric. Forest Meteorol. 149, 1015–1021.

Xiao, J.F., Zhuang, Q.L., Law, B.E., Chen, J.Q., Baldocchi, D.D., Cook, D.R., Oren, R., Richardson, A.D., Wharton, S., Ma, S.Y., Martin, T.A., Verma, S.B., Suyker, A.E., Scott, R.L., Monson, R.K., Litvak, M., Hollinger, D.Y., Sun, G., Davis, K.J., Bolstad, P.V., Burns, S.P., Curtis, P.S., Drake, B.G., Falk, M., Fischer, M.L., Foster, D.R., Gu, L.H., Hadley, J.L., Katul, G.G., Roser, Y., McNulty, S., Meyers, T.P., Munger, J.W., Noormets, A., Oechel, W.C., Paw, K.T., Schmid, H.P., Starr, G., Torn, M.S., Wofsy, S.C., 2010. A continuous measure of gross primary production for the conterminous United States derived from MODIS and AmeriFlux data. Rem. Sens. Environ. 114, 576–591.

Xiao, X.M., Hollinger, D., Aber, J., Goltz, M., Davidson, E.A., Zhang, Q., Moore, B., 2004. Satellite-based modeling of gross primary production in an evergreen needleleaf forest. Rem. Sens. Environ. 89, 519–534.

Yang, F.H., Ichii, K., White, M.A., Hashimoto, H., Michaelis, A.R., Votava, P., Zhu, A.X., Huete, A., Running, S.W., Nemani, R.R., 2007. Developing a continental-scale measure of gross primary production by combining MODIS and AmeriFlux data through Support Vector Machine approach. Rem. Sens. Environ. 110, 109–122.

Zhang, Q., Middleton, E.M., Cheng, Y.-B., Landis, D.R., 2013. Variations of foliage Chlorophyll fAPAR and foliage non-chlorophyll fAPAR (fAPAR$_{chl}$, fAPAR$_{non-chl}$) at the harvard forest. IEEE J. Selected Top. Appl. Earth Observ. Rem. Sens. 6, 2254–2264.

Zhang, Q., Middleton, E.M., Gao, B.-C., Cheng, Y.-B., 2012. Using EO-1 hyperion to simulate HyspIRI products for a coniferous forest: the fraction of PAR absorbed by Chlorophyll (fAPARchl) and leaf water content (LWC). IEEE Trans. Geosci. Rem. Sens. 50, 1844–1852.

Zhao, M., Running, S., 2010. Drought-induced reduction in global terrestrial net primary production from 2000 through 2009. Science 329, 940–943.